J Therm Anal Calorim (2014) 115:567–572
DOI 10.1007/s10973-013-3232-y

Performance of birnessite-type manganese oxide in the thermal-catalytic degradation of polyamide 6

Erdal Eren · Murat Guney · Bilge Eren · Huseyin Gumus

Received: 1 August 2012 / Accepted: 29 April 2013 / Published online: 7 June 2013

Abstract Birnessite-type manganese oxide (BMO) was prepared by oxidation of $Mn(NO_3)_2$ with H_2O_2 in KOH solution. The nature and the extent of degradation of polyamide 6 (PA6) in the presence of samples were analysed by thermogravimetric analysis under static air atmosphere at several heating rates between 5 and 30 °C min^{-1}. The surface and structure of BMO were characterized using infrared (IR) spectroscopy, X-ray diffraction, and thermal analysis techniques. The acid sites of BMO were investigated by IR using pyridine as a molecular probe. The activation energy for degradation estimated by Kissinger method for PA6 and BMO/PA6 system containing 10 mass% of BMO was found to be 212 and 144 kJ mol^{-1} under air, respectively. The catalytic activity observed in BMP catalyst was associated to a high lattice oxygen mobility.

Keywords: Surface acidity · Polyamide 6 · Catalytic degradation · Birnessite · MnO_2

Introduction

Degradation of polymers have drawn attention in the area of thermal degradation because of their importance in the conversion of waste polymers to useful chemical or fuels. Degradation of polymer by non-catalytic thermal method requires high temperatures and produces heavy products. Thermal catalytic degradation yields a much narrower product distribution of carbon atom number and reducing the reaction temperature [1]. Due to this reasons, thermal catalytic degradation of polymeric materials is regarded as the most promising method to realize commercial use [2–5].

The chemical reutilization of polyamide 6 is economically interesting because of the high value of polyamide 6. The addition of a catalyst not only improves the quality of products obtained from degradation of polyamides, but also enables a given selectivity to a certain product to be achieved. It has been found that the main route of thermal degradation of PA6 is the formation of ε-caprolactam (Scheme 1) [6, 7]. The synthesis of the monomer ε-caprolactam proceeds via a complex multi-stage process. Therefore, the recovery of ε-caprolactam from waste polyamide 6 has the potential to be economically competitive with the traditional synthesis process.

Manganese oxides exhibited considerable activity in oxidation–reduction reactions due to the presence of manganese ions with different oxidation states [8–10]. The high activity of manganese oxides was explained in terms of the lattice oxygen mobility [11–15]. The strong correlation between labile lattice oxygen mobility and catalytic activity suggests that the reaction could proceed via the Mars Van Krevelen mechanism [16–19]. According to the Mars-van Krevelen mechanism, organic molecules adsorbed on catalyst surface are oxidized by surface lattice oxygen species. The resultant oxygen vacancies, which would act as active centers in oxidation reactions, are subsequently replenished by oxygen in an air stream during catalytic performance experiments. A careful analysis of the existing literature indicates that not many studies have been conducted at understanding the catalytic thermal

Electronic supplementary material The online version of this article (doi:10.1007/s10973-013-3232-y) contains supplementary material, which is available to authorized users.

E. Eren (✉) · M. Guney · B. Eren · H. Gumus
Department of Chemistry, Faculty of Science and Arts, Bilecik Seyh Edebali University, 11210 Bilecik, Turkey
e-mail: erdaleren16@yahoo.com

Scheme 1 The intra- and intermolecular routes to generate ε-caprolactam

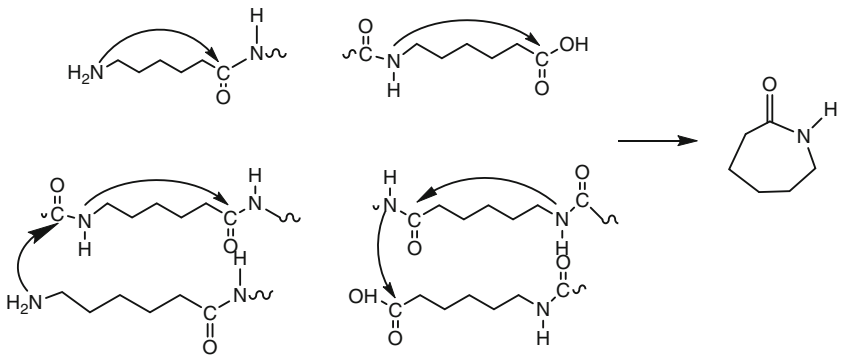

degradation pathway of PA6 using manganese oxides. Taking into account this background, K-rich birnessite-type manganese oxide (BMO) was synthesized and evaluated in the catalytic thermal degradation of PA6. Also, the acid sites of samples were investigated by IR spectroscopy technique using pyridine as a molecular probe.

Experimental

Materials and sample preparation

PA6 pellets used in this study were obtained commercially from Resinex. Other chemicals were of >99.9 % purity or of analytical grade, and purchased from Sigma-Aldrich Co., and used without further purification. Double distilled water was used throughout the experiments.

K-rich BMO was prepared by oxidation of $Mn(NO_3)_2$ with H_2O_2 in KOH solutions. Accordingly, first 2 M (mol L^{-1}) H_2O_2 and 0.6 M (mol L^{-1}) KOH solutions were mixed and stirred in glass beaker. The molar ratio of KOH/H_2O_2 was adjusted as 0.18. After that, immediately manganese solution was poured into the mixture. After the completion of bubbles formation, black precipitate was filtered. Obtained soil was put into the Teflon-lined autoclave and kept at 120 °C for 6 h in 2 M KOH solution. As a final step, the obtained gray precipitate was filtered and washed with deionized water until to obtain neutralization. Several IR absorption bands were observed at 3,412, 1,633, 1,384, 1,066, 622, 602, and 513 cm^{-1}, respectively. Two strong IR bands could be observed around 513 and 602 cm^{-1}, in good agreement with the IR characteristic bands of birnessites.

Characterization techniques

Infrared (IR) spectra of the samples were recorded in the region 4,000–450 cm^{-1} on a a Spectrum-100 FTIR spectrometer. The thermal gravimetric (TG) and differential thermal analyses (DTA) curves were obtained using a PRIS Diamond TG/DTG apparatus under highly pure nitrogen atmosphere.

Surface acidity study

Sample was dried in a hot air oven for 24 h at 120 °C before pyridine treatment for IR measurements. The sample (50 mg) was poured loosely into a sample cup. The loosely filled sample was brought in contact with the pyridine (0.1 cm^3) directly. Then the sample cup was kept in a hot air oven at 100 °C for 1 h to remove physisorbed pyridine. After cooling down to room temperature and adsorption of pyridine, the sample adsorbed pyridine was evacuated for 20 min at several temperatures (120–500 °C). Specimens for measurement were prepared by mixing 0.9 mg of the sample powder with 70 mg of KBr and pressing the mixture into a pellet.

Thermal degradation of PA6

The manganese oxide/PA6 composite was prepared by dissolving stoichiometric amounts of PA6 and manganese oxide in formic acid. The mixture was heated at 40 °C until complete dissolution was achieved. The solution was then cast onto a glass substrate followed by a slow evaporation of the formic acid in a fume hood, then in a vacuum oven at room temperature for 48 h. The thermal decomposition studies in the TG were performed over a temperature range of 50–1,000 °C under both static air environment at different heating rates of 5, 10, 15, 20, 25, and 30 °C min^{-1}.

Results and discussion

Surface acidity of catalysts

The IR spectra in the spectral region 1,400 and 1,700 cm^{-1} after pyridine treatment and thermal desorption at different temperatures for 20 min of pyridine adsorbed on BMO was presented in Fig. 1. The IR absorption bands were

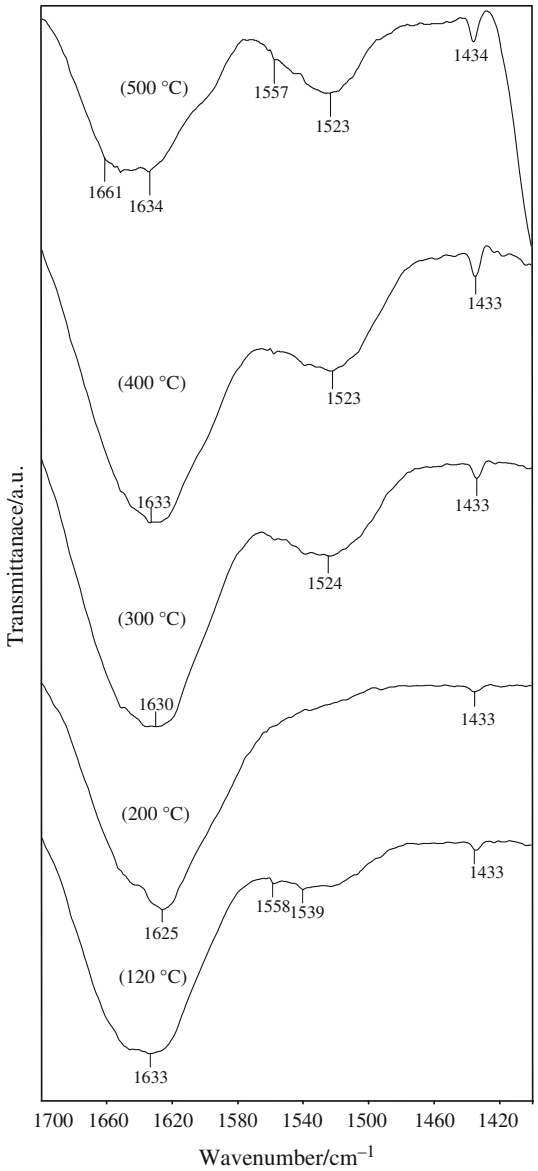

Fig. 1 Desorption of pyridine at different temperatures from BMO surface

assigned according to literature [20–22]. The infrared absorption maxima were measured at 1,433, 1,539, 1,558, 1,633, and 1,646 cm^{-1}, after desorption of pyridine on BMO at 120 °C. The bands observed at 1,539 and 1,558 cm^{-1} indicated the presence of Brønsted acid sites. In Fig. 1a, the attention should be focused on the high-temperature region because at low temperatures, the information about the Lewis sites is obscured by the band of hydrogen-bonded pyridine. The band at 1,434 cm^{-1} was stable to heating at 500 °C. This result indicated that this band was not assignable to hydrogen-bonded pyridine on BMO, which was unstable to outgassing at temperature as low as 120 °C [21, 22]. This band was attributed to the ring-stretching vibration of pyridine coordinately bonded to the Lewis acid centers. After heating at 120 °C, the very broad band observed near 1,633 cm^{-1} included vibration of water and interaction of pyridine with the Lewis sites. It was observed in general that the Lewis-type acidity of the sample was not much affected by heating at higher temperature while Brønsted acid centers practically disappeared. For example, the intensities of the bands assigned to pyridine adsorbed on Lewis site at 1,434 and 1,634 cm^{-1} were still significant, after heating at 500 °C. After heating at 200 °C, the bands at 1,539–1,558 cm^{-1} related with Bronsted acid center were not observed clearly. Upon heating at 300 °C, new broad band at 1,524 cm^{-1} was observed, which do not correspond to known vibrational bands of adsorbed pyridine. Their presence may suggest decomposition of the pyridine.

Thermal-catalytic degradation behavior of PA6

TG and DTG curves for PA6, BMO/PA6 containing 5 % of BMO (5 %-BMO/PA6) and BMO/PA6 containing 10 % of BMO (10 %-BMO/PA6) systems were shown in Figs. 2 and 3. The curve related to the BMO exhibited mass losses by 10.5 and 7.2 % in temperature ranges 20–200 and 200–1,000 °C, respectively (Fig. 2). The mass loss of 3.3 % between 250 and 600 °C was due to the loss of oxygen atoms from the octahedral layer framework in relation to the partial reduction of Mn^{4+} to Mn^{3+} [23, 24], whereas the mass gain centered at 410 and 621 °C was attributed to subsequent oxidation of some Mn^{3+} to Mn^{4+} [25]. The maximum thermal decomposition temperatures of neat PA6, 5 %-BMO/PA6, and 10 %-BMO/PA6 systems were 448, 431, and 402 °C, respectively (Fig. 3). These results implied that the thermal stability of PA6 significantly decreased as the mass percentage of BMO increased. When 50 % mass loss was chosen as a point of comparison, the decomposition temperatures were 436, 418, and 407 °C for neat PA6, 5 %-BMO/PA6 and 10 %-BMO/PA6 systems, respectively. The results revealed that BMO could act as an effective catalyst for reducing the degradation temperature of PA6. The mass of residue retained at 700 °C was found almost proportional to the BMO contents in the PA6 matrix. The high activity of the BMO in thermal oxidation reaction of PA6 was attributed to the solid state charge transfer redox system: Mn^{4+}–$O^{2-}$$Mn^{4+}$↔ Mn^{3+}–□–Mn^{3+}+O_2 (□ representing an oxygen vacancy). The highly reducible bridge oxygen in the Mn^{4+}–O^{2-}–Mn^{4+} couple reacted with PA6 to produce volatile products and a partially reduced Mn^{3+}–□–Mn^{3+} couple. The oxygen vacancy, which would act as active centers in oxidation reactions, was reoxidized rapidly by O_2 in the air atmosphere.

The thermo-oxidative degradation activation energies of samples were calculated by Kissinger method [26] according

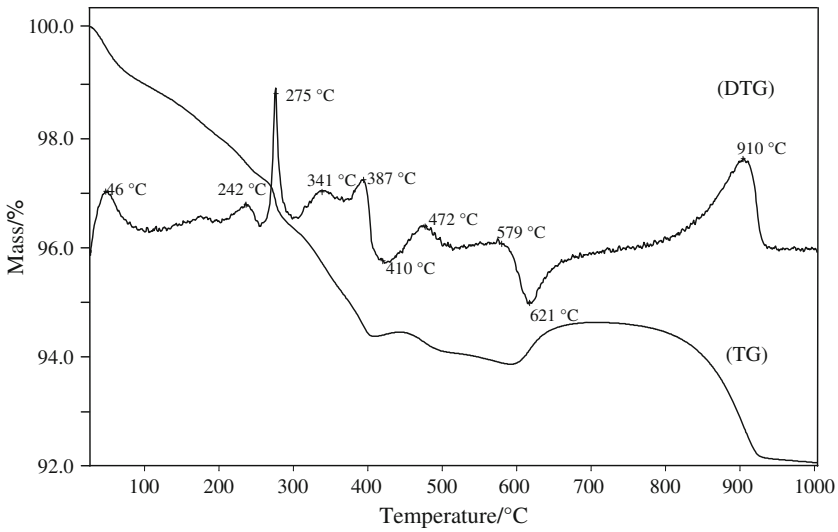

Fig. 2 TG and DTG curves of BMO at a heating rate of 10 °C min^{-1} in static air atmosphere

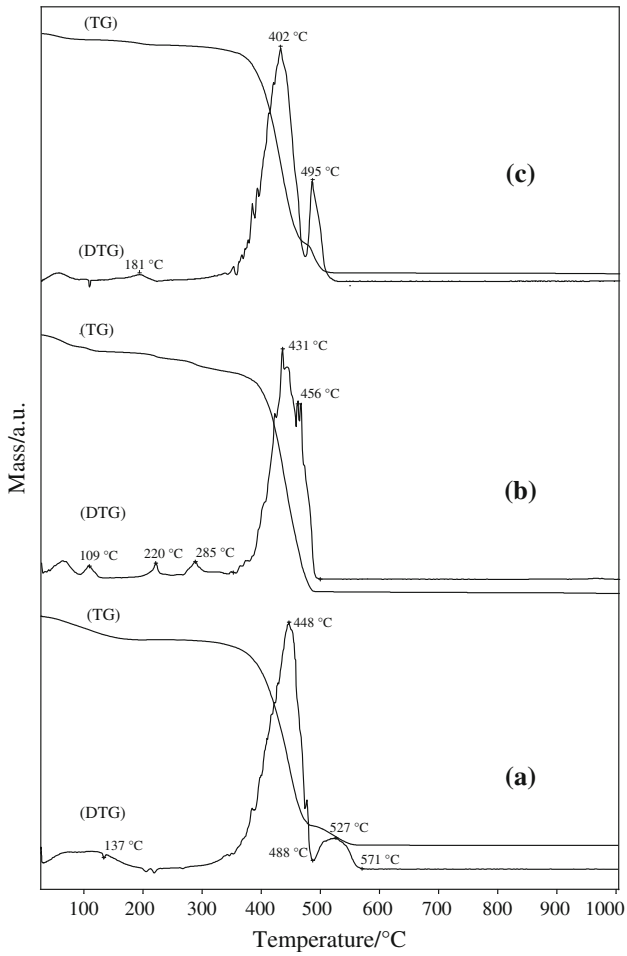

Fig. 3 TG and DTG curves of PA6 (**a**), 5 %-BMO/PA6 (**b**), and 10 %-BMO/PA6 (**c**) systems obtained at a heating rate of 10 °C min^{-1} in static air atmosphere

to the TG data, which were measured under air at different heating rates: 5, 10, 15, 20, 25, and 30 °C min^{-1}. The activation energy for PA6, 5 %-BMO/PA6, and 10 %-BMO/PA6 systems was calculated from the linear dependence of the $\ln\left(\beta/T_{max}^2\right)$ versus $1/T_{max}$ plot (not shown) for various heating rates according to Eq. (1).

$$\ln\left(\frac{\beta}{T_{max}^2}\right) = \left\{\ln\frac{AR}{E_a}\right\} - \frac{E_a}{RT_{max}} \quad (1)$$

In the above equation, A is the pre-exponential factor, E_a is the apparent activation energy of the degradation reaction, R is the universal gas constant, and β is the heating rate. The activation energy was calculated from the T_{max}, the temperature at which the maximum degradation occurs for different heating rates by assuming that mass loss percentage at T_{max} is constant. The E_a values for neat PA6, 5 %-BMO/PA6, and 10 %-BMO/PA6 systems were found to be 212 and 144 kJ mol^{-1} under air, respectively.

Thermal-catalytic degradation mechanism of PA6

In order to understand the interaction between PA6 and BMO, IR spectra were recorded in the range of 4,000–650 cm^{-1} (Fig. 4). The IR spectra of 5 %-BMO/PA6 and 10 %-BMO/PA6 systems were similar to that of PA6. In the spectrum of the PA6 sample, important polyamide bands were observed at 3,292 (N–H stretching), 3,063 (N–H in-plane bending), 1,638 (Amide I), 1,535 (Amide II), 2,942 (CH_2 stretching), and 2,870 cm^{-1} (CH_2 stretching). N–H stretching and Amide I bands strongly depend on hydrogen bonding interactions between the PA6 chains. The amide group is potentially a bi-functional electron donor with 2 sp^2 "lone pairs" at the oxygen atom and a $2p_z^2$ "lone pair" at the nitrogen atom, and therefore it has two possible electron-donating sites to coordinate with the manganese cations. Overlap of $2p_z$ orbitals of the oxygen, carbon, and nitrogen atoms in the planar amide group would reduce the electron density on the nitrogen

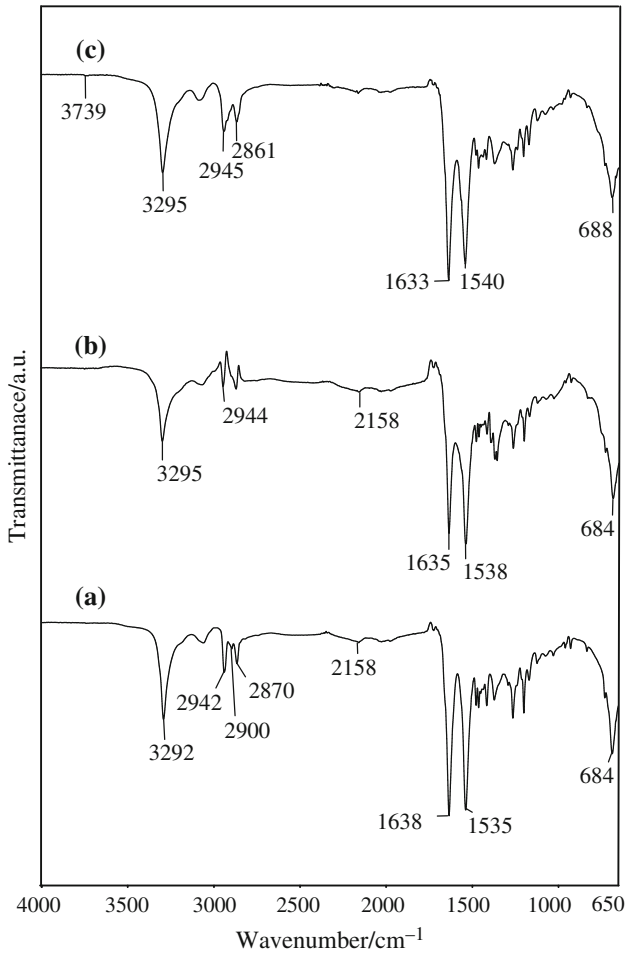

Fig. 4 IR spectra for PA6 (**a**), 5 %-BMO/PA6 (**b**), and 10 %-BMO/PA6 (**c**) systems

atom, and favor the coordination of the manganese ion with the carbonyl oxygen atom. The N–H band at 3,292 cm^{-1} was shifted to 3,295 cm^{-1} in 5 %-BMO/PA6 system suggested that hydrogen bonding is significantly weaker in the BMO/PA6 compared with neat PA6. The C=O band at 1,638 cm^{-1} was shifted to 1,635 cm^{-1} in the 5 %-BMO/PA6 system. This observation suggested that Lewis acid complexation occured on the carbonyl oxygen rather than on the amide group nitrogen. Manganese cation coordination resulted to breaking of the hydrogen bonds between PA6 chains (Scheme 2).

The IR spectra of BMO sample at different temperatures in the range from 1,100 to 450 cm^{-1} were shown in Fig. S1 (Appendix A; see electronic supplementary material, ESM). The bands in the region between 450 and 750 cm^{-1} were assigned to Mn–O vibrations [27–33]. The band located at 522 cm^{-1} were ascribed to the Mn–O bending vibration of [MnO_6] octahedra in BMO sample [28, 32]. The intensity of the Mn–O band was proportional to the content of active oxygen [33]. After heating at 500 °C, the

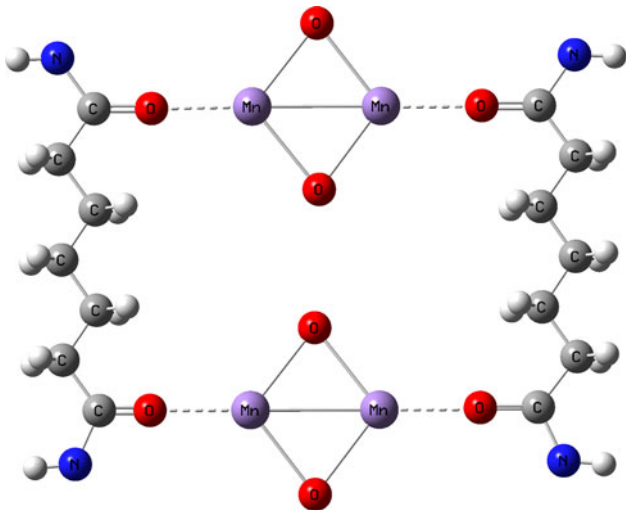

Scheme 2 Breaking of the hydrogen bonds between PA6 chains after BMO addition

peak at 522 cm^{-1} for the BMO sample shifted to 533 cm^{-1} in BMO sample. It was an evidence for the decrease of the surface Mn–O bond strength. Also the increase of the width of the same band in BMO was another confirmation of the the ionic feature of the bond. This results indicated that heating process influenced the mobility of the reacting oxygen.

Conclusions

The results revealed that BMO sample was an effective catalyst for reducing the degradation temperature of PA6. From pyridine desorption studies, it was found that acid sites of BMO were predominantly Lewis acidic in nature. The onset and end-point temperatures of the initial stage TG curve for the BMO systems were decreased. It was clearly observed that the the activation energies of the thermal degradation for the BMO systems was less than that of the neat PA6. The vibrations of the Mn–O bond on the surface of BMO sample indicated the presence of active oxygen. The intensity of the indicated band was proportional to the content of active oxygen.

References

1. Panda AK, Singh PK, Mishra DK. Thermolysis of waste plastics to liquid fuel: a suitable method for plastic waste management and manufacture of value added products—A world prospective. Renew Sust Energ Rev. 2010;14:233–48.
2. Gaur MS, Singh PK, Suruchi, et al. Structural and thermal properties of polysulfone–ZnO nanocomposites. J Therm Anal Calorim. 2013;111:743–51.

3. Lomakin SM, Dubnikova IL, Shchegolikhin AN, et al. Thermal degradation and combustion behavior of the polyethylene/clay nanocomposite prepared by melt intercalation. J Therm Anal Calorim. 2008;94:719–26.
4. Fernandes VJ, Araujo AS, Fernandes GJT, et al. Kinetic parameters of polymer degradation by SAPO-37. J Therm Anal Calorim. 2001;64:585–9.
5. Fernandes VJ, Araujo AS, Medeiros RA, et al. Kinetic parameters of polyethylene degradation by the natural zeolite chabazite. J Therm Anal Calorim. 1999;56:1279–82.
6. Davis RD, Gilman JW, VanderHart DL. Processing degradation of polyamide 6/montmorillonite clay nanocomposites and clay organic modifier. Polym Degrad Stab. 2003;79:111–21.
7. Jang BN, Wilkie CA. The effect of clay on the thermal degradation of polyamide 6 in polyamide 6/clay nanocomposites. Polymer. 2005;46:3264–74.
8. Liu B, Thomas PS, Ray AS, et al. DSC characterisation of chemically reduced electrolytic manganese dioxide. J Therm Anal Calorim. 2007;88:177–80.
9. Szumera M, Waclawska I. Thermal study of Mn-containing silicate-phosphate glasses. J Therm Anal Calorim. 2011;108:583–8.
10. Dose WM, Donne SW. Kinetic analysis of gamma-MnO_2 thermal treatment. J Therm Anal Calorim. 2011;105:113–22.
11. Fakhreia A, Sagheer A, Zaki MI. Synthesis and surface characterization of todorokite-type microporous manganese oxides: implications for shape-selective oxidation catalysts. Microporous Mesoporous Mater. 2004;67:43–52.
12. Cai LN, Guo Y, Lu AH, Branton P, Li WC. The choice of precipitant and precursor in the co-precipitation synthesis of copper manganese oxide for maximizing carbon monoxide oxidation. J Mol Catal A Chem. 2012;360:35–41.
13. Jothiramalingam R, Viswanathan B, Varadarajan TK. Synthesis, characterization and catalytic oxidation activity of zirconium doped K-OMS-2 type manganese oxide materials. J Mol Catal A Chem. 2006;252:49–55.
14. Sun M, Yu L, Ye F, Diao G, Yu Q, Hao Z, Zheng Y, Yuan L. Transition metal doped cryptomelane-type manganese oxide for low-temperature catalytic combustion of dimethyl ether. Chem Eng J. 2013;220:320–7.
15. Zhı K, Lıu Q, Zhang Y, He S, He R. Effect of precipitator on the texture and activity of copper-manganese mixed oxide catalysts for the water gas shift reaction. J Fuel Chem Technol. 2010;38:445–51.
16. El-Shobaky GA, El-Shobaky HG, Badawy AA, Fahmy YM. Physicochemical, surface and catalytic properties of nanosized copper and manganese oxides supported on cordierite. Appl Catal A Gen. 2011;409–410:234–8.
17. Yadav GD, Mewada RK. Selectivity engineering in the synthesis of value added chemicals: oxidation of 1-octanol to 1-octanal over nano-fibrous Ag–OMS-2 catalysts. Chem Eng Res Des. 2012;90:86–97.
18. Baldi M, Finocchio E, Pistarino C, Busca G. Evaluation of the mechanism of the oxy-dehydrogenation of propane over manganese oxide. Appl Catal A Gen. 1998;173:61–74.
19. Doornkamp C, Ponec V. The universal character of the Mars and Van Krevelen mechanism. J Mol Catal A Chem. 2000;162:19–32.
20. Reedy CR, Nagendrappa G, Prakash BSJ. Surface acidity study of Mn+-montmorillonite clay catalysts by ft-ır spectroscopy: correlation with esterification activity. Catal Commun. 2007;8:241–6.
21. Shimizu K, Higuchi T, Takasugi E, Hatamachi T, Kodama T, Satsuma A. Characterization of Lewis acidity of cation-exchanged montmorillonite K-10 clay as effective heterogeneous catalyst for acetylation of alcohol. J Mol Catal A Chem. 2008;284:89–96.
22. Figueiredo FCA, Jordão E, Landers R, Carvalho WA. Evaluation of some supports to RuSn catalysts applied to dimethyl adipate hydrogenation. Appl Catal A Gen. 2009;371:131–41.
23. Liu L, Feng Q, Yanagisawa K, Bignall G, Hashida T. Lithiation reactions of Zn- and Li-birnessites in non-aqueous solutions and their stabilities. J Mater Sci. 2002;37:1315–20.
24. Malankar H, Umare SS, Singh K, Sharma M. Room temperature synthesis of Li-doped MnO_2 and its electrochemical activity. J Solid State Electrochem. 2010;14:71–82.
25. Gaillot AC, Lanson B, Drits VA. Structure of birnessite obtained from decomposition of permanganate under soft hydrothermal conditions. 1. Chemical and structuralvolution as a function of temperature. Chem Mater. 2005;17:2959–75.
26. Kissinger HE. Reaction kinetics in differential thermal analysis. Anal Chem. 1957;29(11):1702–6.
27. Yuan J, Liu ZH, Qiao S, Ma X, Xu N. Fabrication of MnO_2-pillared layered manganese oxide through an exfoliation/reassembling and oxidation process. J Power Sources. 2009;189:1278–83.
28. Ramalingam K, Kamatchi T, Sumod PA. Synthesis, spectral, thermal and CO_2 absorption studies on birnessites type layered MnO_6 oxide. Transit Met Chem. 2006;31:429–33.
29. Liang S, Teng F, Bulgan G, Zong R, Zhu Y. Effect of phase structure of MnO_2 nanorod catalyst on the activity for CO oxidation. J Phys Chem C. 2008;112:5307–15.
30. Li L, Pan Y, Chen L, Li G. One-dimensional α-MnO_2: trapping chemistry of tunnel structures, structural stability, and magnetic transitions. J Solid State Chem. 2007;180:2896–904.
31. Kang L, Zhang M, Liu Z-H, Ooi K. IR spectra of manganese oxides with either layered or tunnel structures. Spectrochim Acta A. 2007;67:864–9.
32. Julien CM, Massot M, Poinsignon C. Lattice vibrations of manganese oxides: part I. periodic structures. Spectrochim Acta A. 2004;60:689–700.
33. Christoskova S, Stoyanova M. Catalytic oxidation of cyanides in an aqueous phase over individual and manganese-modified cobalt oxide systems. J Hazard Mater. 2009;165:690–5.